Palaeogeography, Palaeoclimatology, Palaeoecology 680 (2025) 113331

Contents lists available at ScienceDirect

Palaeogeography, Palaeoclimatology, Palaeoecology

journal homepage: www.elsevier.com/locate/palaeo

# Biomechanical assessment and the fossil record suggest a sensory function in the anterior glabellar and genal spines in Ordovician raphiophorid trilobites

Iván Dario Gómez-Rodríguez [a], Matheo López-Pachón [b], Jorge Esteve [c,*]

[a] Departamento de Ingeniería Mecánica, Universidad de los Andes, Bogotá, Colombia
[b] Departament d'Enginyeria Mecànica, Universitat Rovira i Virgili, Tarragona, Spain
[c] Departamento de Geodinámica, Estratigrafía y Paleontología, Facultad de CC. Geológicas, Universidad Complutense de Madrid, Madrid, Spain

ARTICLE INFO

Editor: L Angiolini

*Keywords:*
Computational fluid dynamic
Ordovician
Trilobites
Behaviour
Palaeoecology

ABSTRACT

Raphiophorid trilobites were small, abundant, and diverse Ordovician trilobites. One of the most remarkable features of these blind trilobites was a spine projecting from the anterior part of the glabella. The discovery of rows of *Ampyx* in the Ordovician of Morocco suggests that the function of this structure may have been related either to enhancing hydrodynamics or to acting as a sensory organ in conjunction with the genal spines. However our results using computational fluid dynamics (CFD) have shown that the spine did not provide any hydrodynamic advantage to these animals. Instead, the shape of the cephalon and body alone was sufficient to prevent them from being dislodged from the seafloor by water currents. The CFD simulations combined with new evidence from the fossil record, of various raphiophorid cuticular structures, suggest that the anterior glabellar and genal spines functioned as a sensory organ. This adaptation likely helped these blind trilobites interact with conspecifics and maintain their orientation in their environment.

## 1. Introduction

Raphiophorid trilobites are diminutive sightless arthropods characterized by a prominent glabella, which is forward-projecting and swollen towards the anterior and often feature a spine in the anteromedian region or a tubercle in a comparable position (Fortey, 1975; Whittington, 1959). Glabellar protrusions, snouts or glabellar "noses" aimed at mitigating surface turbulence have been identified in several actively swimming trilobites (Fortey, 1985). However, in these instances, the remaining exoskeletal morphology diverges significantly from that of raphiophorids. *Microparia*, for instance, exhibits enlarged ocular structures and a streamlined body, along with a condensed thoracic region and a pygidium characterized by robust muscular development. These features strongly suggest pelagic adaptations. Recent analysis using computational fluid simulations further support this morphological interpretation (Esteve and López-Pachón, 2023). Conversely, raphiophorids exhibit atrophy of visual organs, dorsoventral flattening, and diminished musculature, with their distribution seemingly correlated with substrate composition (Vannier et al., 2019; Whittington, 1959). Furthermore, while certain morphological features may superficially appear hydrodynamically advantageous in raphiophorids, such as the balloon-like structures of *Bulbaspis* or the erect spines observed in *Ampyx* and *Lonchodomas* species, they can fail to optimize fluid dynamics. Alternative hydrodynamic functions of spines, such as augmenting drag to facilitate enhanced velocity gradients during filter feeding, cannot be discounted. Nonetheless, such effects are primarily observed in diminutive planktonic organisms (<0.5 mm in length; Emlet and Strathman, 1985), but the hydrodynamic function of spines has not been assessed in trilobites, which typically range in size from 10 to 30 mm. Differences in body size result in distinct oceanic flow regimes due to variations in Reynolds number (*Re*). While microplankton operate at low Reynolds numbers, dominated by viscous forces, larger organisms like raphiophorids experience higher Reynolds numbers, where inertial forces become relevant and flow can be transitional or turbulent. As a result, hydrodynamic mechanisms observed in microplankton, such as viscous-mediated interactions, may not apply to larger arthropods like raphiophorids.

Among the common genera within raphiophorids are *Ampyx* and *Lonchodomas*, which have a broad geographic distribution encompassing regions such as Morocco, the Czech Republic, China, France,

* Corresponding author.
*E-mail address:* jorgeves@ucm.es (J. Esteve).

https://doi.org/10.1016/j.palaeo.2025.113331
Received 3 February 2025; Received in revised form 3 October 2025; Accepted 8 October 2025
Available online 10 October 2025

**Table 1**
Reynolds number for cluster of individuals of *Lonchodomas*.

| *k. Viscosity [m2/s]* | *9.80E-07* |
|---|---|
| *Length [m]* | 0.0473 |
| Velocity [m/s] | Reynolds number |
| 0.3 | 14,487 |
| 0.65 | 31,388 |
| 1 | 48,290 |

Sweden, and the USA (Fortey et al., 2022; El Hassani et al., 1988; Lee et al., 2016; Mansson, 2000; Månsson, 1995; Vannier et al., 2019). These trilobites typically possess elongated anterior glabellar and genal spines. Notably, *Ampyx* specimens often gather in communal clusters within the Fezouata Shale of Morocco during the Lower Ordovician epoch (upper Tremadocian-Floian, approximately 480 million years ago), forming queues. This study investigates the hydrodynamic attributes of these trilobites through computational fluid dynamics (CFD) simulations, examining two distinct scenarios: i) an analysis of an individual specimen and ii) an evaluation of queues comprising two and three individuals; furthermore, we assess the influence of the elongated anterior glabellar spine. The results and the fossil evidence allow us to discuss the putative function of this bizarre structure.

## 2. Material and methods

### 2.1. Fossils

*Ampyx*. The anterior spine in *Ampyx* is long and slender, tapering gradually, distally upturned, and with a rounded cross-section. For this study, 20 complete or nearly complete specimens, with varying degrees of articulation were examined. The specimens represents both internal and external molds, and are preserved in shales and limestones from the Middle Ordovician of Swden. All specimens are housed at the Swedish Museum of Natural History (NRM-PZ), Stockholm, Sweden.

*Lonchodomas*. The anterior spine in *Lonchodomas* possesses a prismatic cross-sectional shape, with the glabella frequently extending towards it, forming a spear-like structure. An enrolled specimen from the National Museum of Prague (NMP), Czech Republic, from Sarka Formation (Middle Ordovician Czech Republic), and two cephalons preserved in limestone (Middle Ordovician, Sweden), housed at the Swedish Museum of Natural History (NRM-PZ-Ar), were utilized for this study.

*Raphioampyx*. *R. argentinus* Baldis and Pöthe-Baldis, 1995, exhibits

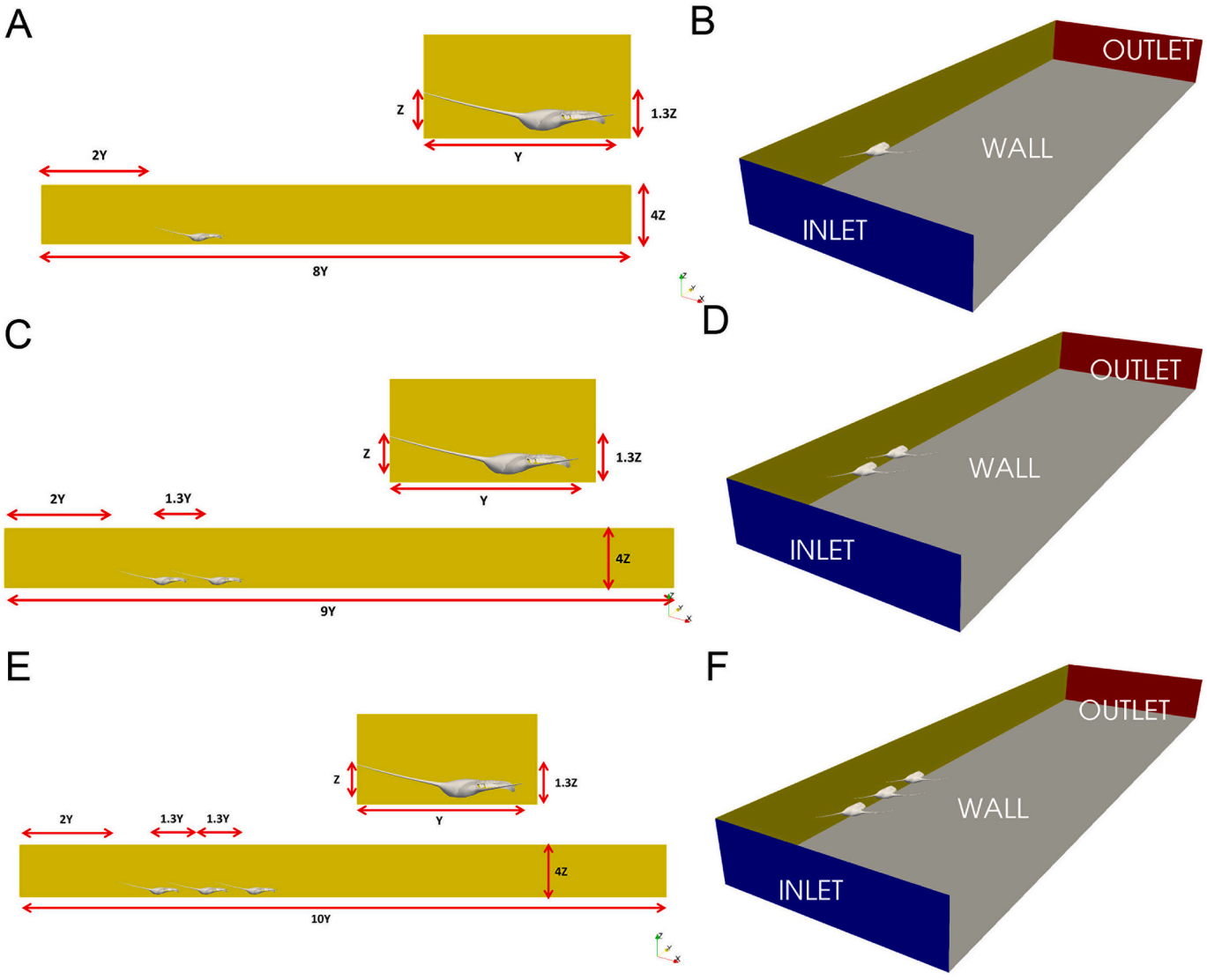


**Fig. 1.** 3D model of *Lonchodomas* based on specimen NMP-L15165 housed at the National Museum of Prague and computational domain for simulations with one individual (A-B), two individuals (C-D) and three individuals (E-F).

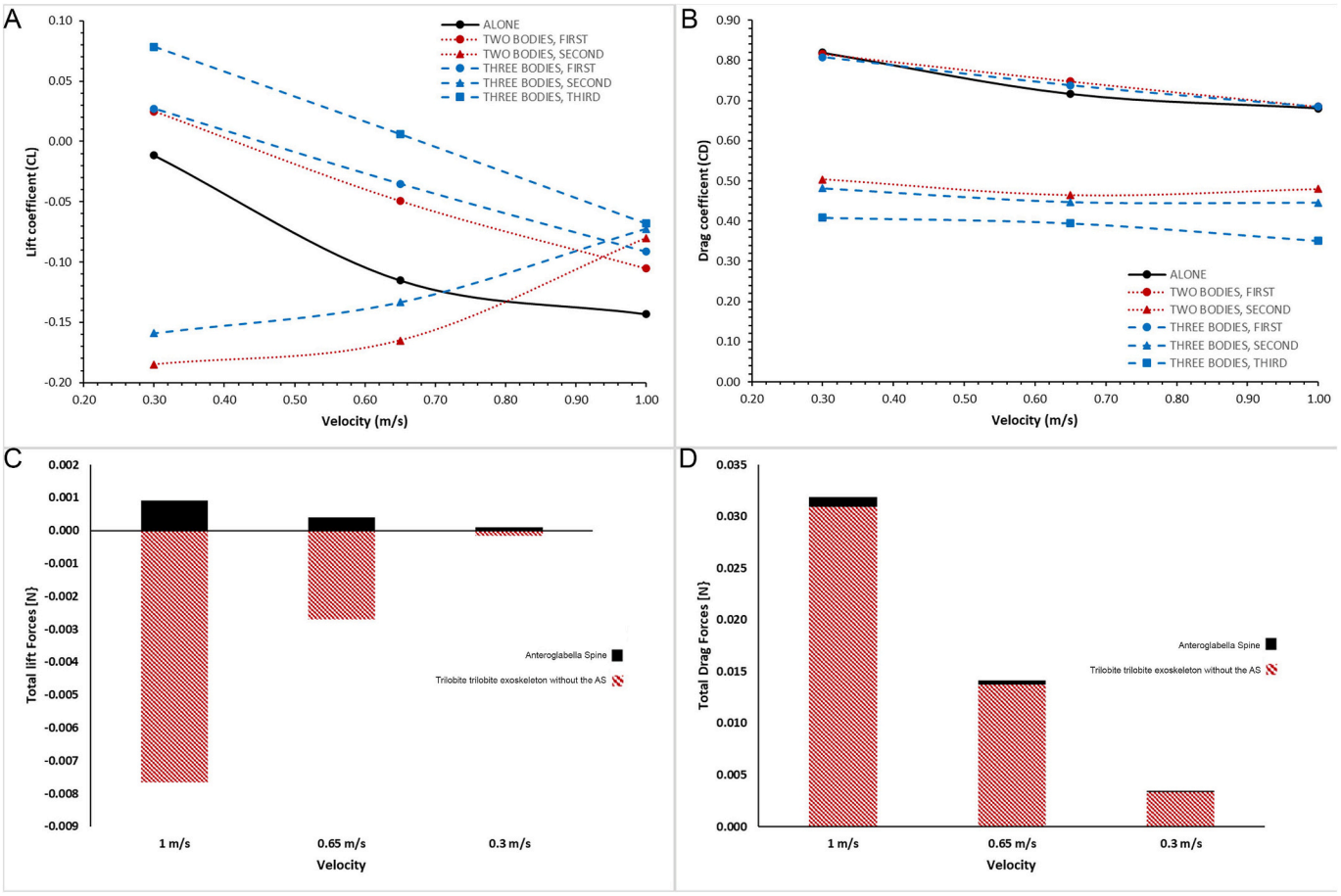


**Fig. 2.** A-B. Lift and drag coefficients. C-D. Total lift and drag forces involving the body or the anterior glabellar spine.

an anterior spine that is elongated and slender, gradually curving upward with a rounded cross-section. Although this taxon was not modelled, nor used for CFD analysis, the preservation of specimens reveals details of the cuticular structure that are significant for discussing the function of the anterior spine. Two specimens were studied: one silicified and one from limestone both from the upper Las Aguaditas Formation (Darriwilian), housed at CICTERRA-CONICET, Córdoba, Argentina.

### 2.2. 3D Models

A three-dimensional digital reconstruction of *Lonchodomas* sp. (NMP-L15165) was produced based on an X-ray microtomography scan of a well-preserved 3D internal mould of the enrolled specimen from the Sarka Formation (Middle Ordovician, the Czech Republic) and housed at the National Museum of Prague. The specimen from the Czech Republic was scanned at the National Museum in Prague using a SkyScan 1172 at 141 μA and 70 kV with Al + Cu Filter. N-Recon Software (Bruker) was used for reconstruction. Two enrolled specimens from the Swedish Museum of the Natural History (NRM-PZ-Ar14122 and NRM-PZ-Ar13397) were scanned at the Museo Nacional de Ciencias Naturales (MNCN) in Madrid, Spain. The specimens from Sweden were scanned using a CT-SCAN- XT H-160 d and VG STUDIO MAX 2.2 was used for reconstruction. The 3D models were developed using Blender, an open-source software (https://www.blender.org/). 3D models include the hypostome on the ventral side of the head (see supplementary information).

### 2.3. Computational fluid simulations

A total of nine water flow simulations around the *Lonchodomas* sp. reconstruction were performed using OpenFOAM V.10. The procedure, as summarized in Esteve et al. (2021a), involved conducting simulations with *Lonchodomas* sp. at varied orientations to the current, facing generally towards the direction of flow, in prone position. These simulations used three flow velocities (0.3 m/s, 0.65 m/s, and 1 m/s, Table 1), which encompass the higher velocities simulated for the locomotion of this trilobite (Esteve and Rubio, 2023) and unstable shallow environments which also correspond with the velocity ranges of near-bottom currents in modern shoreface to offshore environments (Emelyanov, 2005). This velocity range is consistent with the environmental stress proposed by Vannier et al. (2019). The simulations were conducted thrice under identical velocity conditions: once with a single specimen, the second time with two specimens, and finally with three specimens in a row. Drag coefficients stabilize and lift coefficients converge at approximately 1 m/s for groups of two and three individuals, suggesting that the addition of more individuals does not significantly alter the hydrodynamic forces. Limbs were not modelled because their structure is unknown in the fossil state and including them would have unnecessarily complicated the model meshing process and dramatically extended the computational time. To conduct the simulations for the single and row models, three computational domains with refinement boxes around the *Lonchodomas* sp. model were defined, allowing for more accurate simulation of flow in the wake and downstream of the model (Fig. 1). Prism layers were created along the model surface to simulate the viscous effects of the boundary layer; five layers were generated over most of the surface to achieve a y + value of less than 1 for the entire model. The meshing results were highly

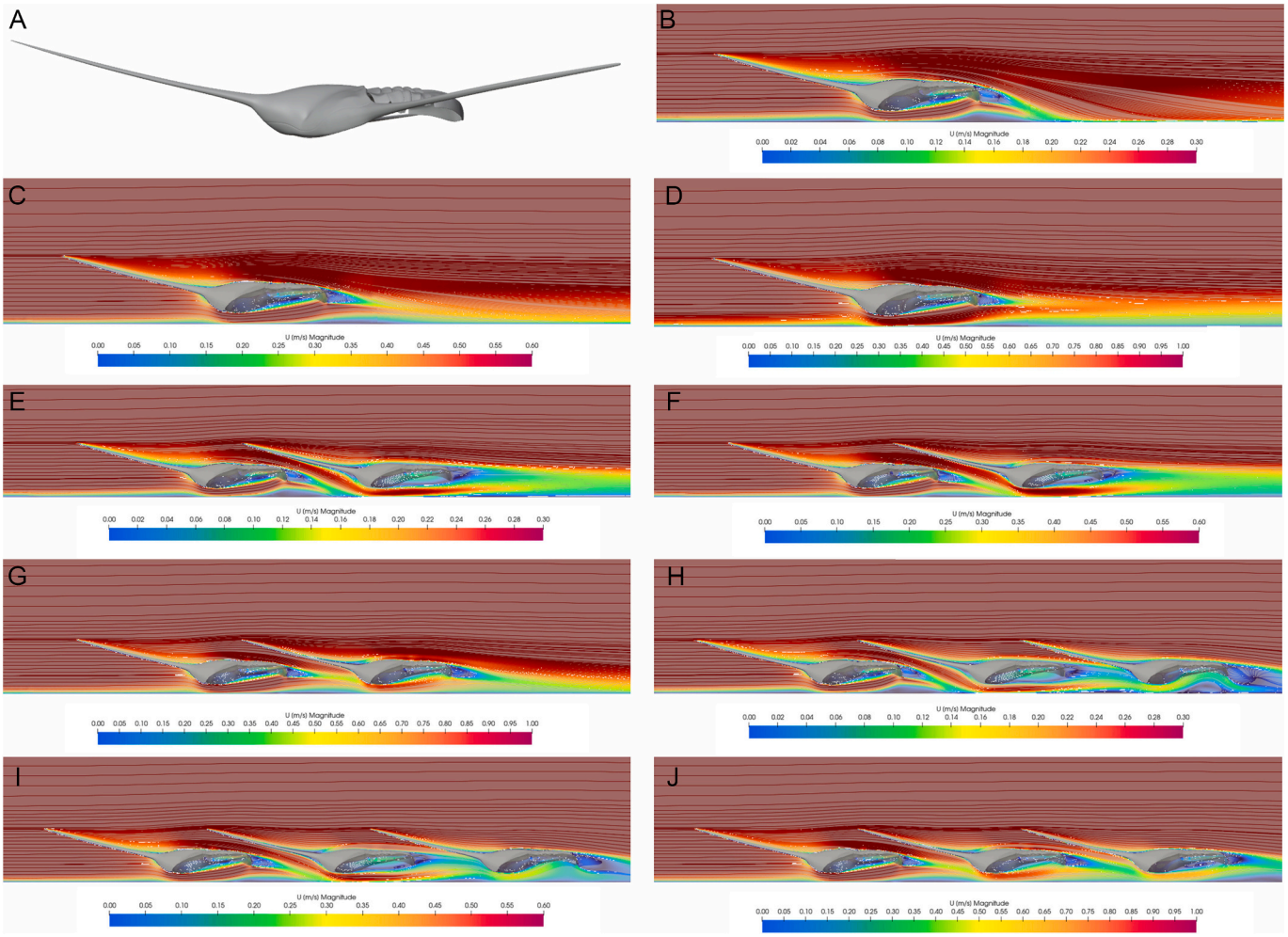


**Fig. 3.** Laterial view of the 3D model of *Lonchodomas* (A). Velocity field for CFD for simulations with one individual (B-D), two individuals (E-G) and three individuals (H-J).

satisfactory, meeting standard quality criteria such as skewness <0.5 (preferably <0.25), aspect ratio < 5, orthogonality >0.1, smooth cell size transitions (growth ratio < 1.2–1.5), and less than 1 for $y^+$ values on the turbulence models. The optimal mesh size was determined through a sensitivity analysis with meshes ranging from approximately 979,047 to 4,382,831 cells. The modelled properties of Ordovician seawater (Esteve et al., 2021a; Lumpkin and Johnson, 2013; Veizer et al., 1997; Veizer and Prokoph, 2015) were used in the simulation, treating the fluid as isothermal, incompressible, and Newtonian, with environmental conditions deduced for the Ordovician period informing the fluid's physical properties (Esteve and López-Pachón, 2023). Given that raphiophorid trilobites (*Lonchodomas*, *Ampyx* and *Raphioampyx*) are interpreted as benthic trilobites (Fortey, 1985; Fortey and Owens, 1999), their legs are assumed to have an average length of 1 mm above the seafloor, corresponding to the re-scaled leg height according to Esteve and Rubio (2023). A moving wall condition with the inlet velocity was applied to the ground. The outlet had a pressure condition equal to barometric pressure. The Reynolds number (Eq. (1)) represents the ratio of viscous forces to inertial forces within a fluid experiencing relative internal movement due to different fluid velocities.

$$R_e = \frac{\rho V L}{\mu} = \frac{V L}{\nu} \tag{1}$$

Where $\rho$ is the fluid density, $V$ is the freestream velocity, $L$ is the characteristic length, and $\mu$ is the dynamic viscosity of the fluid and $\nu$ is the kinematic viscosity of the fluid. The Reynolds number indicates whether a flow is turbulent or laminar. According to the Reynolds numbers of the simulation, ranging from 14,487 to 48,290 (Table 1), and to assess hydrodynamics under stable environmental conditions, the analysis was conducted under laminar flow conditions. However, traditional turbulence models like *SST* $k-\omega$ have problems predicting the fluid behaviour within the transition regime. Therefore, in order to solve this problem, the *Langtry Menter* $k-\omega$ *SST* turbulence model was performed for velocities of 0.3, 0.65, and 1 m/s, following the procedure in Esteve et al. (2021b) and the equations of Langtry and Menter (2009) and Menter (1994). The SIMPLE (Semi-Implicit Method for Pressure-Linked Equations) pressure-based solver was employed for pressure-velocity coupling in the steady simulations.

## 3. Results

### 3.1. Lift coefficient

The lift coefficient is a dimensionless parameter used to quantify the vertical forces exerted by a fluid around an object's geometry. This parameter describes the pressure distribution caused by fluid forces across the object's surface in a flow field. The lift coefficient is mathematically defined in Eq. (2):

$$C_L = \frac{L}{\frac{1}{2}\rho V^2 A} \tag{2}$$

where L is the lift force, ρ is the fluid density, V is the freestream velocity,

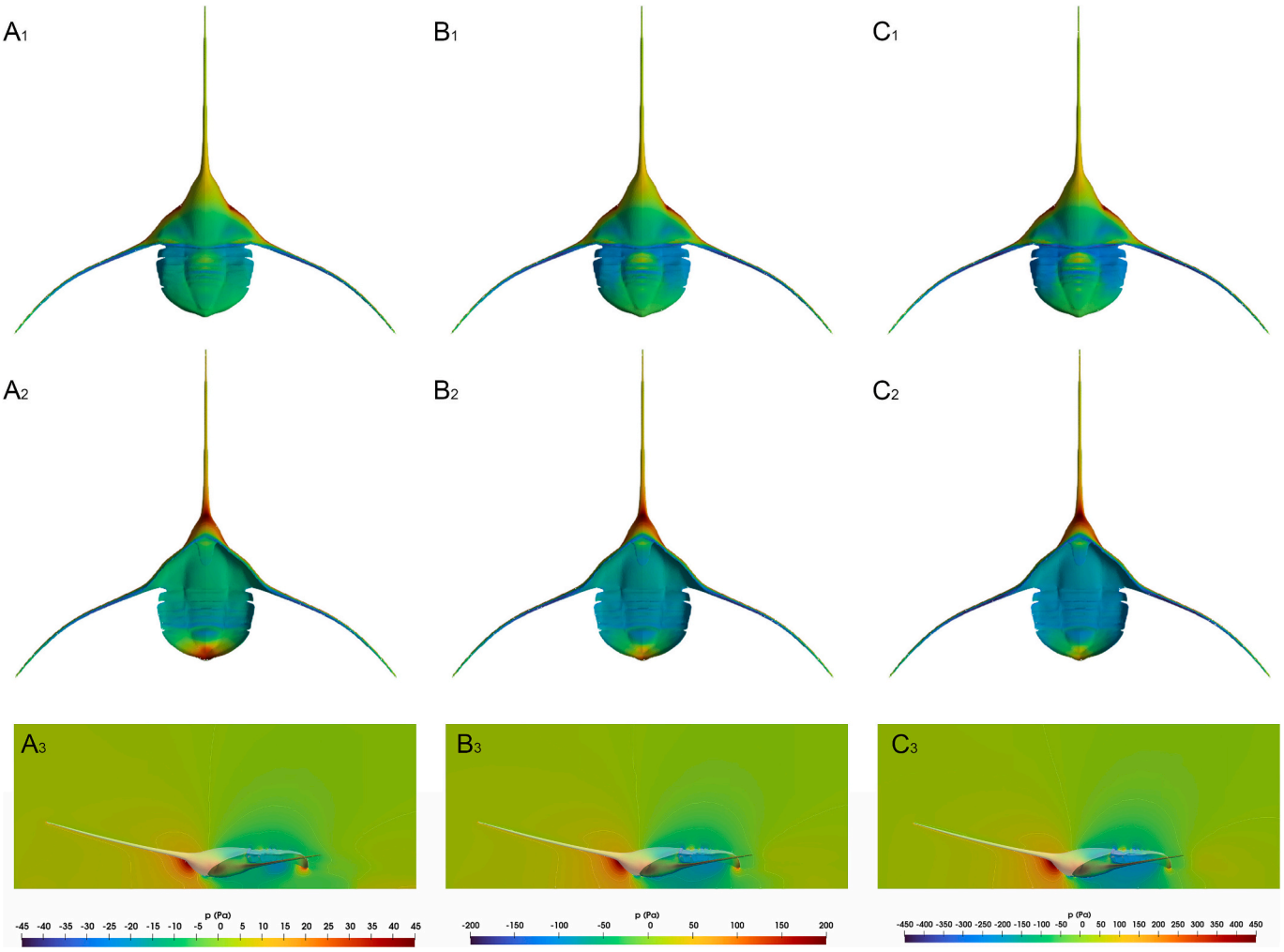


**Fig. 4.** Pressure in CFD simulations with one individual under flow at 0.30 $ms^{-1}$ (A), (A). 0.65 $ms^{-1}$ (B) and 1 $ms^{-1}$ (c).

and A is the cross-sectional area.

The lift coefficient results show that, for the analysed velocity range, this value is mostly negative. This indicates that the specimen's geometry facilitates adhesion to the ground when in motion (Fig. 2A). For the single-specimen model, the trend shows that as flow velocity increases, the lift coefficient becomes more negative. In contrast, in the two-specimen simulations, the second specimen exhibits a lower lift coefficient than the first at low flow velocities, but as flow velocity increases, its lift coefficient also increases, even surpassing that of the first specimen (Fig. 2A). In the three-specimen simulations, the third specimen experiences positive lift at low flow velocities. However, as flow velocity increases, its lift coefficient decreases, eventually reaching values similar to those of the second specimen (Fig. 2A).

### 3.2. Drag coefficients and forces

The drag coefficient is a dimensionless parameter that quantifies the resistance force encountered by an object submerged in a fluid. In trilobites, the fluid corresponds to water flowing around its body. The drag forces result from pressure and friction effects. The drag coefficient is mathematically defined as (Eq. (3)):

$$C_d = \frac{2F_d}{\rho V^2 A} \tag{3}$$

where Fd is the drag force, ρ is fluid density, V is the freestream velocity, and A is the cross-sectional area.

The drag coefficient (Cd) decreases with the increases in boundary velocity for a single individual, this is a typical condition in any fluid simulation due to the squared velocity term in the drag equation. In simulations with two or three specimens, trailing trilobites showed substantial drag reduction compared to the leader (~62–70 %) at all simulated inlet velocities (Fig. 2B). In simulations with two specimens, the first specimen exhibits a trend alike that of the single-specimen simulation. However, the drag coefficient of the second specimen remains nearly constant over the analysed velocity range. A similar trend is observed in the three-specimen simulation (Fig. 2B), where the third specimen in line also experiences a nearly constant drag coefficient. This indicates that the first specimen ensures a reduction in drag for the following specimens, regardless of the analysed velocity range.

### 3.3. Velocity field

The results indicate that flow velocity decreases rapidly upon encountering the raphiophorids model, creating a pronounced velocity gradient (the boundary layer) near the lower and upper margins of the simulation volume. The velocity fields reveal a vortex created beneath the *Lonchodomas* model and a short low-velocity wake that forms downstream of the trilobite (Fig. 3A). Higher flow velocities do not alter the geometry of the vortices or the wake (Fig. 3B-C). In simulations with two specimens, it can be observed that the vortex beneath the body and the wake also form in the leading specimen (Fig. 3D). The wake shape benefits the second specimen, positioning it where velocities shift from

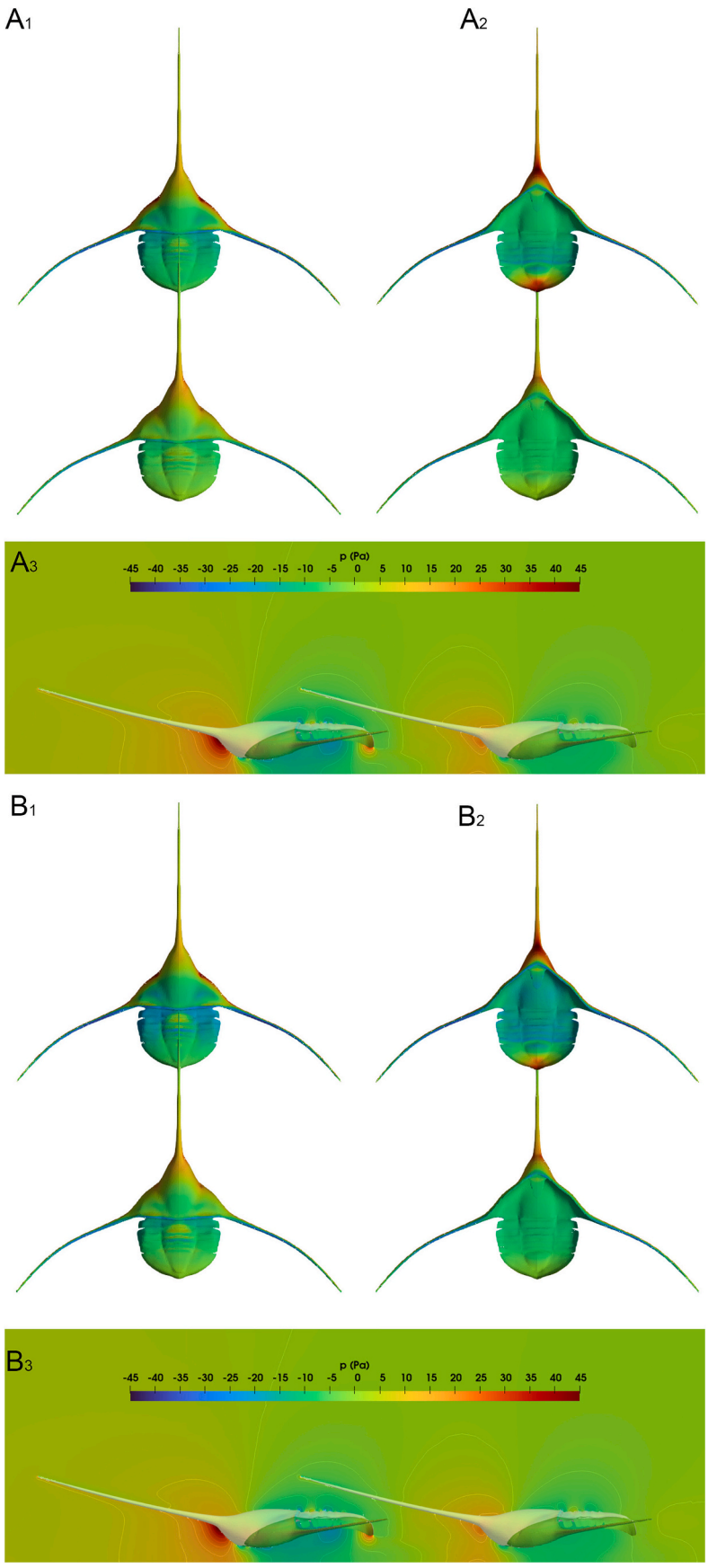


**Fig. 5.** Pressure in CFD simulations with two individuals under flow at 0.30 $ms^{-1}$ (A) and 0.65 $ms^{-1}$ (B).

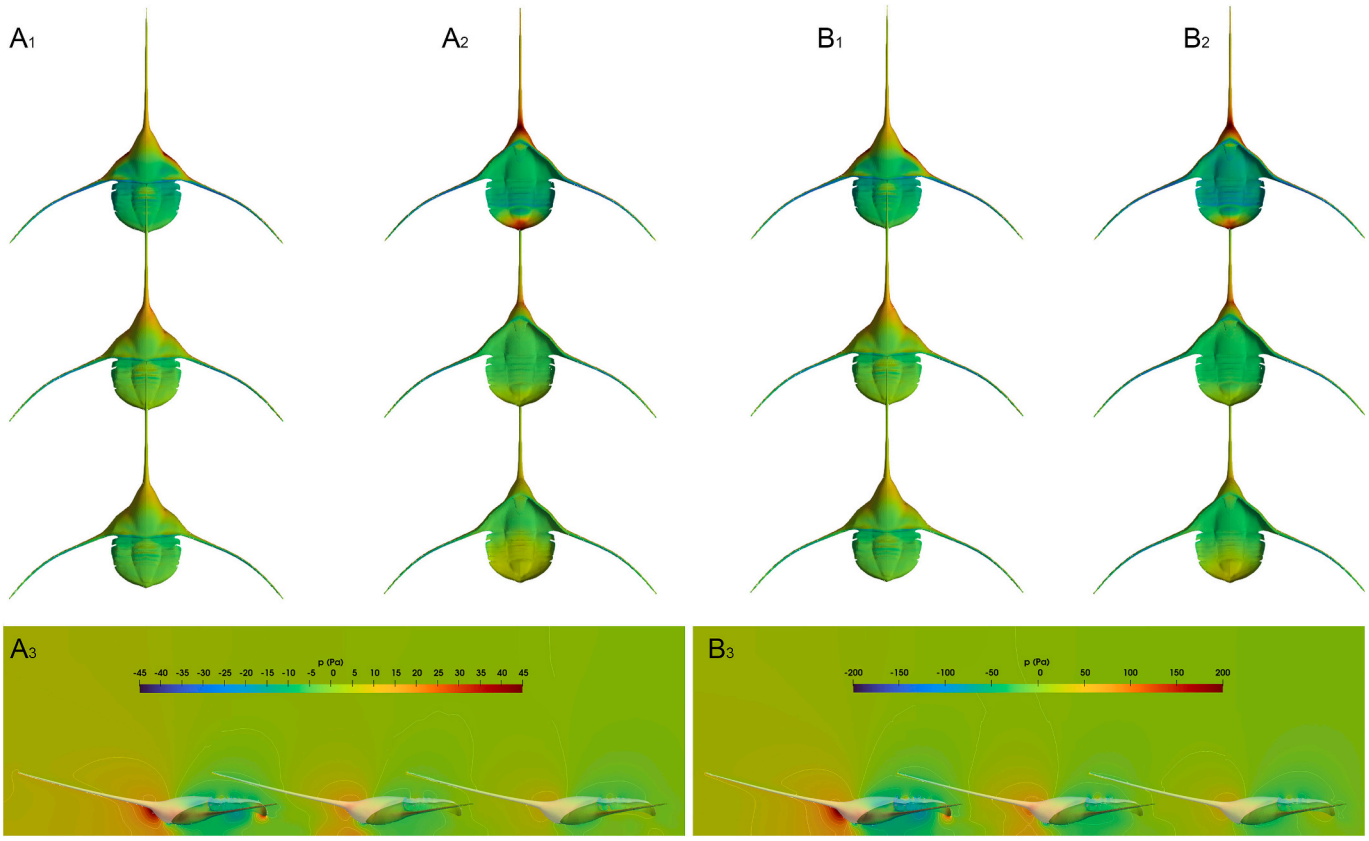


**Fig. 6.** Pressure in CFD simulations with three individuals under flow at 0.30 $ms^{-1}$ (A) and 0.65 $ms^{-1}$ (B).

low to high, just below the anteroglabellar spine (Fig. 3D-E). The second specimen also exhibits velocity fields with a vortex beneath the body of the model and a long, fairly symmetrical low-velocity zone downstream (Fig. 3D). Low flow velocities downstream of the second specimen enable effective positioning the third specimen (Fig. 3G-I). As flow velocity increases in simulations with two specimens, the geometry of the longer wake from the second specimen shifts closer to the seafloor and to the pygidium of the second specimen (Fig. 3E-F). This pattern observed in the two-specimen simulation is repeated when adding a third specimen (Fig. 3G-I). As flow velocity increases, the vortices in all wakes move closer to the trilobite body.

### 3.4. Pressure

In single-specimen *Lochodomas* models, flow velocity was low in the posterior region under frontal flows (Figs. 4–6). The lateral margins of the cephalon, the anterior glabellar lobe on its ventral surface, and the most proximal part of the anteroglabellar spine exhibit highly positive pressures. These regions experience the highest flow velocities. These high pressures are counteracted by negative pressures across much of the cephalon and very negative pressures on the most proximal part of the genal spines. These negative pressures likely prevent the raphiophorid from being dislodged from the seafloor. Relatively negative pressures are observed on both the dorsal and ventral sides of the thorax, with the last two segments experiencing the most negative values. However, very high pressure is also detected at the doublure of the pygidium, related to the vortex formed in that region. This is counterbalanced by the highly negative pressure detected in the last two segments (Fig. 4A). This pressure pattern is repeated at higher flow velocities, except for the positive pressure at the pygidial doublure, which decreases in area, becoming a single point at 1 m/s (Fig. 4B-C). In simulations with two and three specimens, positive pressures on the ventral cephalon decrease significantly in the second and third specimens at higher velocities. Similarly, the positive pressure on the pygidial doublure disappears entirely at lower velocities (Figs. 5A-B-6A-B).

## 4. Discussion

The functions and potential roles of certain trilobite structures have been extensively debated over the last century. Initially, these discussions relied solely on fossil evidence, as exemplified by studies on enrolment (e.g., Bergström, 1973; Esteve et al., 2011) or vision (e.g. Clarkson et al., 2006). Later, more robust lifestyle interpretations emerged by combining morphological traits, even inferring evolutionary characteristics within different groups (Clarkson, 1969; Hammann, 1983). A critical source for interpreting trilobite ecology is the fossil record itself. Combined with morphology, and through approaches such as biogeography or biostratinomic studies, it has been possible to describe pelagic lifestyles (Fortey, 1985) or synchronized moulting behaviours (Corrales-García et al., 2020). However, many functional interpretations remain speculative, relying on subjective analyses that require validation through modern techniques (e.g. Bicknell et al., 2018; Esteve et al., 2021b; Esteve and López-Pachón, 2023; Shiino et al., 2014; Shiino et al., 2012).

Vannier et al. (2019) provided a detailed description of an assemblage comprising multiple individuals of the raphiophorid *Ampyx* from the Lower Ordovician of Morocco. In the clusters described, the specimens were aligned in a row, with their long anteroglabellar and genal spines sometimes touching the dorsal surface of the trilobite ahead and behind them. By integrating this fossils data with sedimentological data from the outcrop where these trilobites were found, the authors concluded that this collective behaviour likely arose in response to a biological reproductive signal or synchronization for moulting, as described by (Corrales-García et al., 2020). Vannier et al. (2019) further proposed, drawing analogies from studies of modern lobsters, that the

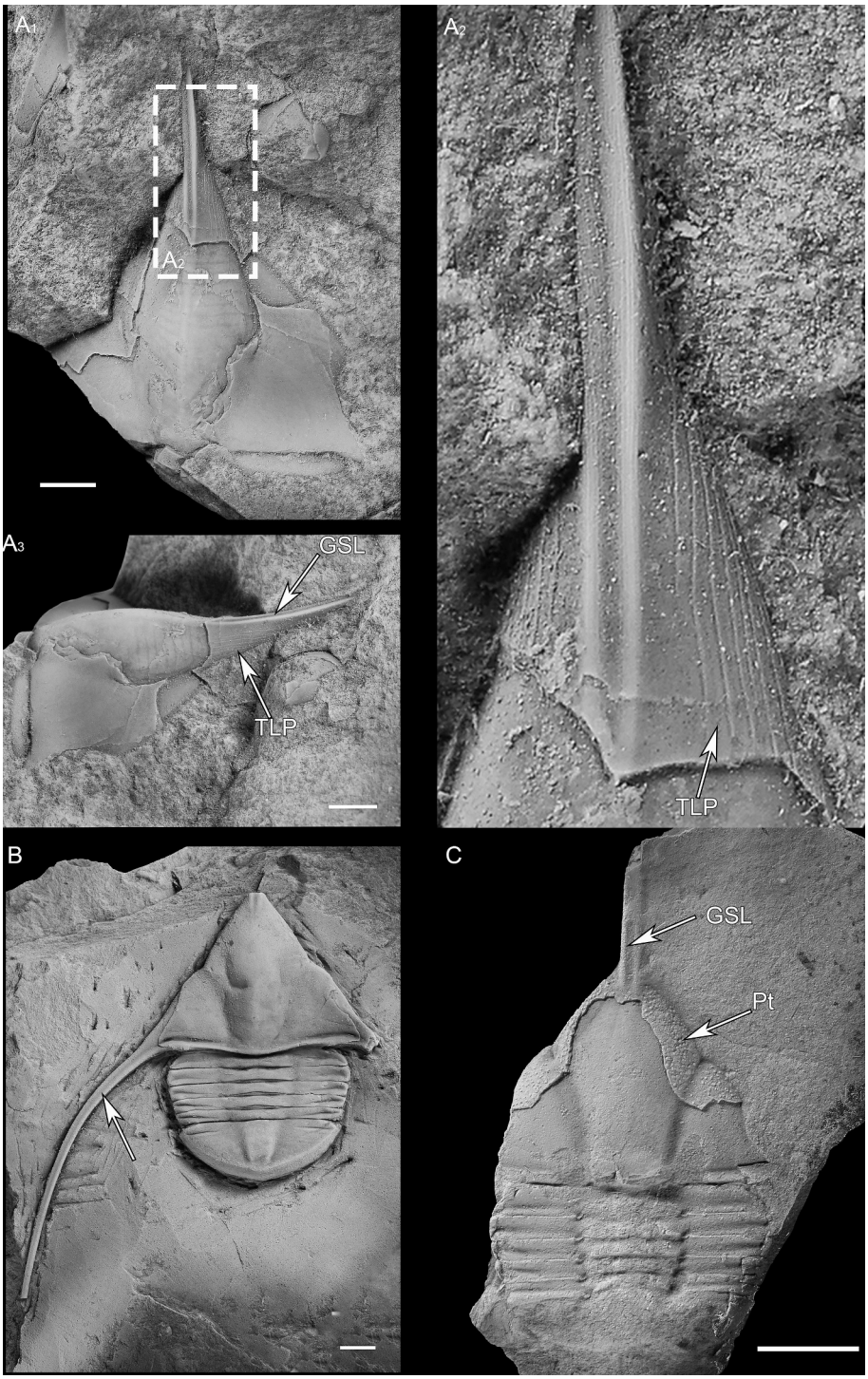


**Fig. 7.** A. *Lonchodomas* sp. (SMNH-Ar71016), $A_1$ Dolsal view; $A_2$ Detail of A1; $A_3$. Lateral view., B. *Ampyx portlocki* Barrande, 1852 (SMNH-Ar14206); C. *Ampyx tetragonus* Angelin, 1878 (SMNH-Ar14151). GAS: Groove of anterior glabellar spine; FGS, furrow of the genal spina; TLP: terrace lines and pits and Pt: pits.

alignment reduced drag, providing an energetic advantage for migration, wherever the individuals were headed.

Our CFD simulations reveal that the drag on the leading individual remains constant, irrespective of flow velocity or longer queue of individuals. However, adding more individuals to the queue significantly reduces the drag of the following trilobites, providing a clear migratory advantage. A slightly different trend is observed in lift forces. Lift decreases at higher flow velocities, preventing trilobites from being lifted off the seafloor. Trilobites with positive lift can be detached from the seafloor (Esteve et al., 2021a), which, in the case of *Ampyx,* is not an appropriate ecological strategy since an effective collective behaviour requires individuals to remain closely grouped together. The lift experienced by the second and third individuals is very high at lower flow velocities but becomes negative as the flow velocity increases. This effect is noteworthy, as highly negative lift values at high velocities could improve trilobite movement. Although drag and lift coefficients are influenced by the number of individuals and vary in each specimen along the queue, it is still important to understand the extent to which the elongated anteroglabellar spine influences the hydrodynamic performance of these raphiophorids. The CFD simulations presented here

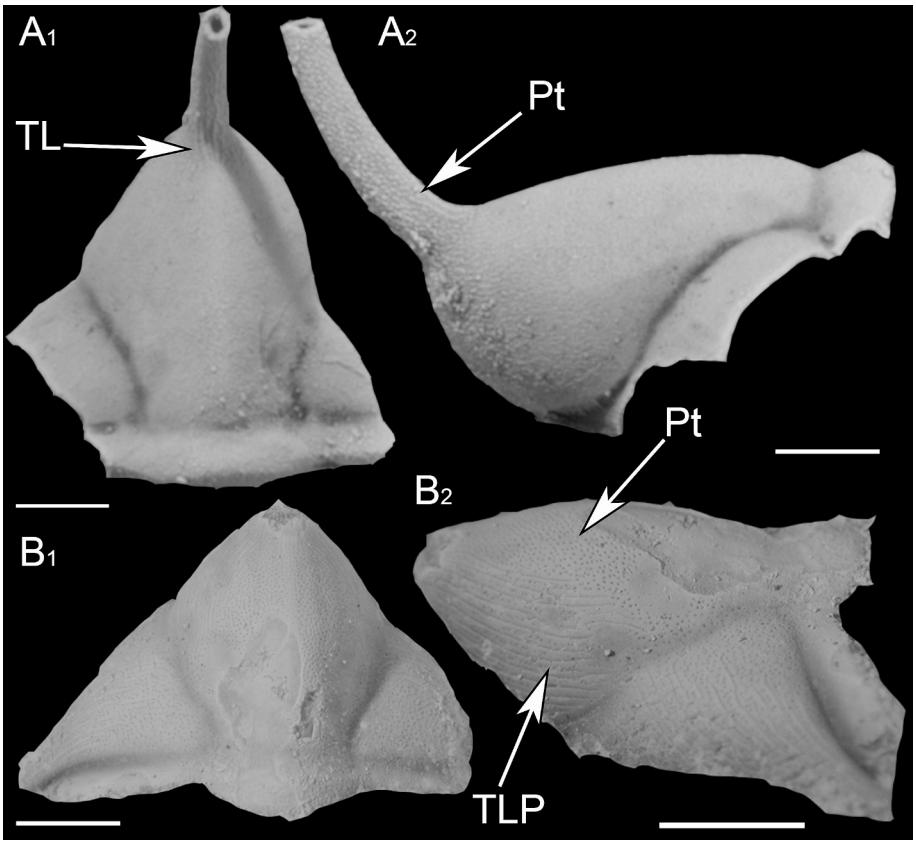


**Fig. 8.** *Raphioampyx argentinus* Baldis and Pöthe-Baldis, 1995 (CONICET). TLP: terrace lines and pits and Pt: pits.

allow us to isolate this specific morphological feature from the rest of the exoskeleton and assess its direct contribution to both drag and lift generation. This approach provides a clearer understanding of the functional significance of the spine in the context of hydrodynamic efficiency. Fig. 2C shows the integrated forces averaged in the direction parallel to the flow for two separate parts of the trilobite exoskeleton (i.e. anterior glabellar spine and the body itself) while the Fig. 2D shows the integrated forces averaged in the direction perpendicular to the flow for these two separate parts of the trilobite exoskeleton. In both cases, the percentage of force (i.e. drag and lift forces) corresponding to the anterior glabellar spine is negligible compared to the rest of the exoskeleton. Thus, CFD simulations show that the anterior glabellar spine has no significant impact on drag or lift coefficients (Fig. 2C-D). Furthermore, the analysis of velocity fields and pressure coefficients reveals that the cephalon's morphology primarily contributes to the stabilization of trilobites on the seafloor, with no discernible effect from the glabellar spine. Consequently, the hypothesis that the glabellar spine served as a hydrodynamic stabilization structure can be rejected. Instead, it is the specific morphology of the cephalon and fixigena that enhances the trilobite's stability.

Wang et al. (2024) analysed the effects of the wake in trilobite queues and suggested that if a trilobite moved outside the wake, the asymmetric field of velocity and pressure helped it reposition itself, thereby facilitating the maintenance of migratory queues. This allowed blind trilobites to reliably detect their companions, compensating for their lack of vision, at low speeds (i.e., during locomotion). However, our results show that the wake effect would be lost at speeds above 0.35 m/s (see Fig. 3D-E, F-G, I-J), while fluctuations in the pressure fields of the rear part of the trilobite trunk could still be detectable by the anteroglabellar spine, allowing trilobites to maintain migratory queues even at high-speed regimes when the wake becomes shorter (see Figs. 4–5). Nevertheless, not all blind raphiophorids possess these long glabellar spines (e.g., *Globampyx* or *Ampyxinella*), and some even exhibit ocular structures (e.g., *Lehnertia nawisapa*). If the anteroglabellar spine functions to detect pressure fluctuations at high flow velocities, this could explain why cases like the raphiophorid *Ampyxinella* are found "displaced" within clusters from the Lower Ordovician (Upper Tremadocian–Floian) Saint-Chinian Formation in the Montagne Noire (see Vannier et al., 2019, Fig. SM13). However, at low flow velocities, the wake may still have allowed them to position themselves within the queue in this and other cases (Hanchen et al., 2021; Trenchard et al., 2017). Based on the observed stabilization and convergence of drag and lift coefficients at speeds around 1 m/s for groups of two and three individuals, we predict that adding a fourth or fifth individual to the queue would result in minimal changes to these coefficients. This suggests that the wake formed behind the leading individual, although short, becomes sufficiently stable and protective for additional members to experience similar hydrodynamic conditions. In low-speed cases such as that shown by Wang et al. (2024), this makes more sense given that the wake is longest at those speeds. Consequently, the queue likely maintains its hydrodynamic efficiency, with diminishing returns in drag reduction as group size increases. Furthermore, the inclusion of more individuals may contribute to a more continuous and stable wake structure, potentially improving alignment and coordination within the group (see Hanchen et al., 2021; Wang et al., 2024). Overall, these predictions support the idea that the system reaches a hydrodynamic equilibrium where the addition of more individuals does not substantially alter the aerodynamic forces experienced, but may improve group stability and locomotion synchronization. This supports the idea that blind (and non-blind) trilobites may have used these queues for migrations related to moulting or mating, or to achieve greater stability during periods of environmental disturbance such as storms, as we see in the fossil record (Hanchen et al., 2021; Trenchard et al., 2017; Vannier et al., 2019; Wang et al., 2024).

These findings, alongside the morphological traits of *Ampyx*, *Lonchodomas*, and *Raphioampyx argentinus*, provide a framework for

discussing the unique lifestyles of these animals. All three species exhibit terrace lines on their anteroglabellar and genal spines. The anteroglabellar spine often features a medial groove, with terrace lines running along its entire length (Fig. 7). Additionally, pits are present, either aligned along the terrace lines or distributed seemingly irregularly across the dorsal surface of the cephalon (Fig. 8). The discovery of pits and associated canals suggest the presence of sensory setae in trilobites. This mechanoreceptor function is supported by comparisons with modern crustaceans, in which specialized setae serve as current detectors, as observed in the lobster *Homarus* and the crayfish *Procambarus* (Miller, 1975). Terrace lines and pits are also interpreted as sensory organs (Schmalfuss, 1978). However, this interpretation does not exclude a potential role in substrate stabilization (Schmalfuss, 1978; Seilacher, 1985). The fact that the anteroglabellar spine is hollow (Fig. 8A) further supports the sensory organ hypothesis, given that a solid spine would likely hinder the sensory function of the pits and terrace lines. The appearance of this morphological trait (i.e. anteroglabellar spine), unlike other characteristics such as the proposon that develop gradually (see Laibl et al., 2014), occurs abruptly during ontogeny. Raphiophorids like *Lonchodomas* or *Ampyx* undergo a significant metamorphosis between the protaspid stage, with non-adult like larvae and the meraspid stage, where the anteroglabellar spine appears (Brian et al., 1994). Multiple planktonic protaspid instars explain the wide geographic distribution of these trilobites (Laibl et al., 2023). However, the fact that such a rapid metamorphosis occurs, with the anteroglabellar spine already well developed by the M0 stage, highlights the importance of this structure once the organism lives on the benthos. Knell and Fortey (2005) suggested that these spines may have had a hydrodynamic function during the juvenile stages, when body length from M0 to M3 would range between 0.5 and 1.5 mm. Similar spines have been described in modern copepods to increase drag, since their feeding currents operate under viscous forces, that is, at low Reynolds number, assisted by metachronal swimming (Ford et al., 2019; Granzier-Nakajima et al., 2020; Paffenhöfer et al., 1982). This suggests that at least the earliest juvenile stages in these raphiophorids were not strictly benthic but rather nektobenthic, inhabiting the interface between the seafloor and the water surface. They may have been capable of swimming freely in the water column to feed, while also being able to adhere to and move across the substrate, similar to some modern copepods (Bradford-Grieve, 2004; Guidi-Guilvard et al., 2009). Further work is needed to assess this hypothesis. However, once a size threshold is surpassed, viscous forces change and the anteroglabellar spine ceases to affect drag. Instead, it may serve to detect wakes or pressure changes, helping individuals stay aligned in a row under flow conditions of low and especially high velocity.

Evidence from the fossil record showing queues of raphiophorid trilobites (Vannier et al., 2019), and details of their anteroglabellar spine structure, along with CFD analysis, indicates that the anteroglabellar spine may have functioned as a sensory organ. This structure likely helped these blind trilobites maintain orientation during migrations for mating or synchronized moulting but also for navigating through environmentally stressful events, such as severe storms.

## CRediT authorship contribution statement

**Iván Dario Gómez-Rodríguez:** Writing – review & editing, Investigation. **Matheo López-Pachón:** Writing – review & editing, Investigation. **Jorge Esteve:** Writing – review & editing, Writing – original draft, Investigation, Funding acquisition, Conceptualization.

## Declaration of competing interest

We declare no conflict of interest.

## Acknowledgements

We thank Tim Topper and Jonas Hagström (Swedish Museum of the Natural History) for kind access to collections in their care. We also thank Zuzana Hermanová (National Museum, Prague) for her assistance with X-ray micro-tomography and her kind access to collections in her care. Cristina Paradella (MNCN, Madrid) kindly assisted with the X-ray micro-tomography. We are grateful to Emilio Vaccari and Neal Handkamer (CONICET, Córdoba, Argentina) for discussion about raphiophorids and allowing us to use the imagines in Fig. 7. We are grateful to Harriet Drage (University of Lausanne) for her kind revision of an earlier version of this manuscript and for the English proofreading. We thank to Stephen Pates (UCL) and an anonymous reviewer whose valuable suggestions helped improve the original manuscript. This research was supported by the SYNTHESYS Program (SE-TAF-3323), and is a contribution to the projects PID2021-125585NB-I00 and CNS2024-154147 of the Spanish Ministry of Science Innovation and Universities. M.L.C. is supported by the European Union's Horizon 2020 Research and Innovation Programme under the Marie Skłodowska-Curie grant agreement No. 945413 (Marti-Franques COFUND Fellowship).

## Appendix A. Supplementary data

Supplementary data to this article can be found online at https://doi.org/10.1016/j.palaeo.2025.113331.

## Data availability

The authors confirm that all data necessary for supporting the scientific findings of this paper have been provided.

## References

Bergström, J., 1973. Organization, life and systematics of trilobites. Fossils Strata 2, 1–69.

Bicknell, R.D.C., Ledogar, J.A., Wroe, S., Gutzler, B.C., Watson, W.H., Paterson, J.R., 2018. Computational biomechanical analyses demonstrate similar shell-crushing abilities in modern and ancient arthropods. Proc. R. Soc. B Biol. Sci. https://doi.org/10.1098/rspb.2018.1935, 20181935.

Bradford-Grieve, J.M., 2004. Deep-sea benthopelagic calanoid copepods and their colonization of the near-bottom environment. Zool. Stud. 43.

Brian, D.E. Chatterton, Gregory, D. Edgecombe, Stephen, E. Speyer, Allen, S. Hunt, Richard, A. Fortey, 1994. Ontogeny and relationships of Trinucleoidea (Trilobita). J. Paleontol. 68 (3), 523–540. https://doi.org/10.1017/S0022336000025907.

Clarkson, E.N.K., 1969. A functional study of the Silurian Ordontopleurid Trilobite *Leonaspis* deflexa (Lake). Lethaia 2, 329–344.

Clarkson, E., Levi-Setti, R., Horváth, G., 2006. The eyes of trilobites: the oldest preserved visual system. Arthropod Struct. Dev. 35, 247–259. https://doi.org/10.1016/j.asd.2006.08.002.

Corrales-García, A., Esteve, J., Zhao, Y., Yang, X., 2020. Synchronized moulting behaviour in trilobites from the Cambrian Series 2 of South China. Sci. Rep. 10, 14099. https://doi.org/10.1038/s41598-020-70883-5.

El Hassani, A., El Wartiti, M., Zahraoui, M., Destombes, J., Willefert, S., 1988. On the discovery of an Arenigian macrofauna (lower Ordovician) with trilobites and graptolites in the Rabat area, north-western coastal Meseta, Morocco. C. R. Acad. Sci. Ser. II (307), 1589–1594.

Emelyanov, E., 2005. The Barrier Zones in the Ocean. Springer.

Emlet, R.B., Strathman, R.R., 1985. Gravity, drag, and feeding currents of small zooplankton. Science 228, 1016–1017. https://doi.org/10.1126/science.228.4702.1016.

Esteve, J., López-Pachón, M., 2023. Swimming and feeding in the Ordovician trilobite *Microparia speciosa* shed light on the early history of nektonic life habits. Palaeogeogr. Palaeoclimatol. Palaeoecol. 625. https://doi.org/10.1016/j.palaeo.2023.111691.

Esteve, J., Rubio, P., 2023. Understanding locomotion in trilobites by means of three-dimensional models. IScience 26. https://doi.org/10.1016/j.isci.2023.107512.

Esteve, J., Hughes, N.C., Zamora, S., 2011. Purujosa trilobite assemblage and the evolution of trilobite enrollment. Geology 39, 575–578. https://doi.org/10.1130/G31985.1.

Esteve, J., López, M., Ramírez, C.G., Gómez, I., 2021a. Fluid dynamic simulation suggests hopping locomotion in the Ordovician trilobite *Placoparia*. J. Theor. Biol. 531. https://doi.org/10.1016/j.jtbi.2021.110916.

Esteve, J., Marcé-Nogué, J., Pérez-Peris, F., Rayfield, E., 2021b. Cephalic biomechanics underpins the evolutionary success of trilobites. Palaeontology 64, 519–530. https://doi.org/10.1111/pala.12541.

Ford, M.P., Lai, H.K., Samaee, M., Santhanakrishnan, A., 2019. Hydrodynamics of metachronal paddling: effects of varying reynolds number and phase lag. R. Soc. Open Sci. 6, 191387. https://doi.org/10.1098/rsos.191387.

Fortey, R.A., 1975. The ordovician trilobites of spitsbergen II. Asaphidae, nileidae, raphiophoridae and telephinidae of the valhallfonna formation. Nor. Polarinst. 162, 210.

Fortey, R.A., 1985. Pelagic trilobites as an example of deducing the life habits of extinct arthropods. Trans. R. Soc. Edinb. Earth Sci. 76, 219–230. https://doi.org/10.1017/S0263593300010452.

Fortey, R.A., Owens, R.M., 1999. Feeding habits in trilobites. Palaeontology 42, 429–465. https://doi.org/10.1111/1475-4983.00080.

Fortey, R.A., Wernette, S.J., Hughes, N.C., Revision of F. R. C, 2022. Reed's Ordovician trilobite types from Myanmar (Burma) and western Yunnan Province, China. Zootaxa 5162, 301–356. https://doi.org/10.11646/zootaxa.5162.4.1.

Granzier-Nakajima, S., Guy, R.D., Zhang-Molina, C., 2020. A numerical study of metachronal propulsion at low to intermediate reynolds numbers. Fluids 5, 1–15. https://doi.org/10.3390/fluids5020086.

Guidi-Guilvard, L.D., Thistle, D., Khripounoff, A., Gasparini, S., 2009. Dynamics of benthic copepods and other meiofauna in the benthic boundary layer of the deep NW Mediterranean Sea. Mar. Ecol. Prog. Ser. 396, 181–195. https://doi.org/10.3354/meps08408.

Hammann, W., 1983. Calymenacea (Trilobita) aus dem Ordovizium von Spanien; ihre Biostratigraphie, Ökologie und Systematik. Abh. Senckenberg. Naturforsch. Ges. 542, 1–177.

Hanchen, Song, Haijun, Song, Rahman, I.A., Chu, D., 2021. Computational fluid dynamics confirms drag reduction associated with trilobite queuing behaviour. Palaeontology 64, 597–608. https://doi.org/10.1111/pala.12562.

Knell, R.J., Fortey, R.A., 2005. Trilobite spines and beetle horns: sexual selection in the Palaeozoic? Biol. Lett. https://doi.org/10.1098/rsbl.2005.0304.

Laibl, L., Fatka, O., Crônier, C., Budil, P., 2014. Early ontogeny of the cambrian trilobite Sao hirsuta from the Skryje-Týřovice basin, Barrandian area, Czech Republic. Bull. Geosci. 89, 293–309. https://doi.org/10.3140/bull.geosci.1438.

Laibl, L., Saleh, F., Pérez-Peris, F., 2023. Drifting with trilobites: the invasion of early post-embryonic trilobite stages to the pelagic realm. Palaeogeogr. Palaeoclimatol. Palaeoecol. 613, 111403. https://doi.org/10.1016/j.palaeo.2023.111403.

Langtry, R.B., Menter, F.R., 2009. Correlation-based transition modeling for unstructured parallelized computational fluid dynamics codes. AIAA J. 47, 2894–2906. https://doi.org/10.2514/1.42362.

Lee, S.B., Lee, D.C., Woo, J., Zhang, X., 2016. Systematic revision of trilobites from the middle ordovician (darriwilian) klimoli formation of the zhuozishan area, Inner Mongolia, China. Acta Geol. Sin. Engl. Ed. 90, 1955–1975. https://doi.org/10.1111/1755-6724.13015.

Lumpkin, R., Johnson, G.C., 2013. Global Ocean surface velocities from drifters: mean, variance, El Niño-Southern Oscillation response, and seasonal cycle. J, Geophys, Res, Ocean 2992–3006. https://doi.org/10.1002/jgrc.20210.

Månsson, K., 1995. Trilobites and stratigraphy of the Middle Ordovician Killeröd Formation, Scania, Sweden. GFF 117, 97–106. https://doi.org/10.1080/11035899509546206.

Mansson, K., 2000. Dionidid and raphiophorid trilobites from the middle Ordovician (Viruan Series) of Jamtland, Central Sweden. Trans R Soc Edinburgh. Earth Sci. https://doi.org/10.1017/s0263593300002650.

Menter, F.R., 1994. Two-equation eddy-viscosity turbulence models for engineering applications. AIAA J. 32, 1598–1605. https://doi.org/10.2514/3.12149.

Miller, J., 1975. Structure and function of trilobite terrace lines. - Fossils Strata 4, 155–178.

Paffenhöfer, G.A., Strickler, J.R., Alcaraz, M., 1982. Suspension-feeding by herbivorous calanoid copepods: a cinematographic study. Mar. Biol. 67. https://doi.org/10.1007/BF00401285.

Schmalfuss, H., 1978. Structure, patterns and function of cuticular terraces in Recent and fossil arthropods. - Zoomorphologie 90, 19–40.

Seilacher, A., 1985. Trilobite palaeobiology and substrate relationships. Trans. R. Soc. Edinb. Earth Sci. 76, 231–237. https://doi.org/10.1017/S0263593300010464.

Shiino, Y., Kuwazuru, O., Suzuki, Y., Ono, S., 2012. Swimming capability of the remopleuridid trilobite *Hypodicranotus striatus*: Hydrodynamic functions of the exoskeleton and the long, forked hypostome. J. Theor. Biol. 7, 29–38. https://doi.org/10.1016/j.jtbi.2012.01.012.

Shiino, Y., Kuwazuru, O., Suzuki, Y., Ono, S., Masuda, C., 2014. Pelagic or benthic? Mode of life of the remopleuridid trilobite *Hypodicranotus striatulus*. Bull. Geosci. 89, 207–218. https://doi.org/10.3140/bull.geosci.1409.

Trenchard, H., Brett, C.E., Perc, M., 2017. Trilobite 'pelotons': possible hydrodynamic drag effects between leading and following trilobites in trilobite queues. Palaeontology 60, 557–569. https://doi.org/10.1111/pala.12301.

Vannier, J., Vidal, M., Marchant, R., El Hariri, K., Kouraiss, K., Pittet, B., et al., 2019. Collective behaviour in 480-million-year-old trilobite arthropods from Morocco. Sci. Rep. 9. https://doi.org/10.1038/s41598-019-51012-3.

Veizer, J., Prokoph, A., 2015. Temperatures and oxygen isotopic composition of Phanerozoic oceans. Earth-Sci. Rev. 92–104. https://doi.org/10.1016/j.earscirev.2015.03.008.

Veizer, J., Buhl, D., Diener, A., Ebneth, S., Podlaha, O.G., Bruckschen, P., et al., 1997. Strontium isotope stratigraphy: potential resolution and event correlation. Palaeogeogr. Palaeoclimatol. Palaeoecol. 132, 65–77. https://doi.org/10.1016/S0031-0182(97)00054-0.

Wang, Z., Edgecombe, G.D., Hou, J., bo., 2024. Function of flow wakes for queuing trilobites: Positioning rather than drag reduction – Criteria for drag force assessment in palaeontological CFD simulations. Palaeogeogr. Palaeoclimatol. Palaeoecol. 646, 112239. https://doi.org/10.1016/J.PALAEO.2024.112239.

Whittington, H.B., 1959. Silicified Middle Ordovician Trilobites: Remopleurididae, Trinucleidae, Raphiophoridae, Endymioniidae. Bull. Mus. Comp. Zool. 124, 200.